iScience

Article

Tunable exchange bias, magnetoelectric transport and negative thermal expansion in $Mn_3Ni_{1-x}Co_xN$

Graphical abstract

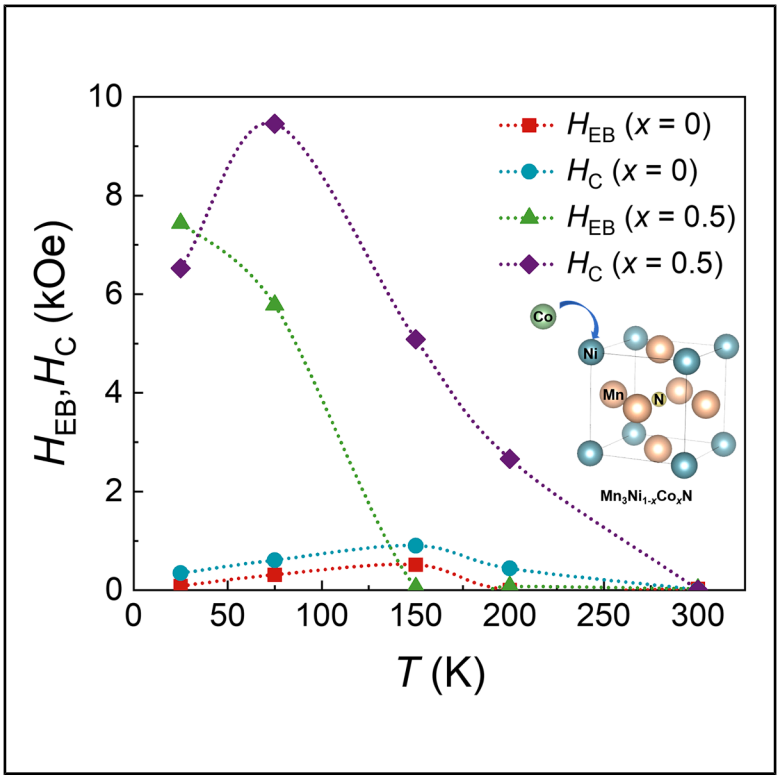

Highlights

- $Mn_3Ni_{1-x}Co_xN$ undergoes an AFM-to-FIM transition with Co doping
- Co-doping strengthens the exchange-bias effect and coercivity in $Mn_3Ni_{1-x}Co_xN$
- Negative thermal expansion is tunable in $Mn_3Ni_{1-x}Co_xN$ through spin-lattice coupling

Authors

Dongmei Hu, Sihao Deng, Ying Sun, ..., Zonglun Li, Le Kang, Cong Wang

Correspondence

dengsh@ihep.ac.cn (S.D.),
kangl@ihep.ac.cn (L.K.),
congwang@buaa.edu.cn (C.W.)

In brief

Materials science; Magnetic property; Materials structure

Hu et al., 2026, iScience *29*, 115300
April 17, 2026
https://doi.org/10.1016/j.isci.2026.115300

CellPress

iScience

CellPress
OPEN ACCESS

Article

Tunable exchange bias, magnetoelectric transport and negative thermal expansion in $Mn_3Ni_{1-x}Co_xN$

Dongmei Hu,[1,2] Sihao Deng,[1,2,*] Ying Sun,[3] Kewen Shi,[4] Christoph Sürgers,[5] Gerda Fischer,[5] Bao Yuan,[1,2] Xudong Shen,[1,2] Dexiang Gao,[1,2] Zonglun Li,[1,2] Le Kang,[1,2,*] and Cong Wang[4,6,7,*]

[1]Spallation Neutron Source Science Center, Dongguan, China
[2]Institute of High Energy Physics, Chinese Academy of Sciences, Beijing, China
[3]School of Physics, Beihang University, Beijing, China
[4]School of Integrated Circuit Science and Engineering, Beihang University, Beijing, China
[5]Physikalisches Institut, Karlsruhe Institute of Technology, Karlsruhe, Germany
[6]National Key Lab of Spintronics, International Innovation Institute, Beihang University, Hangzhou, China
[7]Lead contact
*Correspondence: dengsh@ihep.ac.cn (S.D.), kangl@ihep.ac.cn (L.K.), congwang@buaa.edu.cn (C.W.)
https://doi.org/10.1016/j.isci.2026.115300

SUMMARY

Antiperovskite materials have significant potential in spintronics due to distinctive magnetic and electronic transport characteristics. This work systematically investigates the effects of Co substitution on the magnetic, electronic transport, and thermal expansion properties of $Mn_3Ni_{1-x}Co_xN$. Co substitution triggers a transformation from noncollinear antiferromagnetic to ferrimagnetic ordering. For $x = 0.5$, a pronounced exchange bias is observed, with a maximum exchange bias field of 7.44 kOe at 25 K and coercivity reaching 9.45 kOe at 75 K. This effect significantly modulates the anomalous Hall effect, providing clear evidence for spin-charge coupling in antiperovskites. All samples exhibit negative thermal expansion near magnetic transitions, with coefficients ranging from -65.64×10^{-6} K^{-1} ($x = 0$) to -23.55×10^{-6} K^{-1} ($x = 0.7$), revealing intrinsic correlations between magnetic transitions and lattice dynamics. This work advances the understanding of magnetic ordering mechanisms in antiperovskite materials and provides a basis for designing functional materials with tunable magnetic properties.

INTRODUCTION

Manganese-based antiperovskite compounds Mn_3XN (where X represents transition metals) constitute an emerging class of multifunctional magnetic materials that exhibit tremendous application potential in precision devices, spintronic devices, and magnetic sensors. These compounds adopt a typical cubic crystal structure, wherein transition metal X atoms occupy the corner positions of the cubic lattice, Mn atoms are located at the face-centered positions, and N atoms reside at the body-centered positions. The Mn and N atoms collectively form a distinctive geometrically frustrated Mn_6N octahedral framework structure.[1,2] This unique configuration distinguishes them from conventional magnetic functional metals[3–5] or ceramics and gives rise to pronounced ''spin-lattice-charge'' coupling effects.[6,7] It is precisely this coupling mechanism that leads to their rich variety of physical properties, including magnetovolume effect (MVE)[8,9] with tunable negative/zero thermal expansion (NTE/ZTE),[9–11] near-zero temperature coefficient of resistance (NZ-TCR),[12] giant magnetoresistance,[13] magnetocaloric effect,[14,15] magnetostriction,[16,17] exchange bias (EB),[18,19] and unconventional transport properties induced by non-collinear or non-coplanar spin structures such as anomalous Hall effect (AHE).[20,21]

The microscopic mechanisms underlying the rich physical properties of antiperovskite materials can be understood from the following aspects: First, fine-tuning the valence electron count at the X-site can redistribute the density of states near the Fermi level, and alter the competition between direct Mn - Mn exchange and indirect Mn-N-Mn superexchange interactions,[2,22] thereby enabling synergistic control of multiple magnetic phases including Γ^{5g} type non-collinear antiferromagnetic (AFM), canted AFM,[23] ferromagnetism (FM), and coexisting ferromagnetic-antiferromagnetic (AFM-FM) states.[24] Second, antiperovskite materials exhibit strong ''spin-lattice'' coupling effects.[6] During magnetic ordering transitions, this coupling results in abrupt lattice constant changes and discontinuous isotropic volume contractions, consequently producing pronounced thermal expansion anomalies. Additionally, these magnetic transitions are often accompanied by significant changes in the resistivity.[7] Third, the electronic transport properties of Mn-based antiperovskites, intrinsically linked to their structural and electronic characteristics, lead to various scattering mechanisms, including spin-dependent scattering,[25] electron-phonon scattering, and electron-electron interactions, resulting in distinctive transport phenomena such as resistivity minima, anomalous magnetoresistance, and metal-semiconductor-like transitions.[16,26,27] Therefore, controlling carrier concentration and

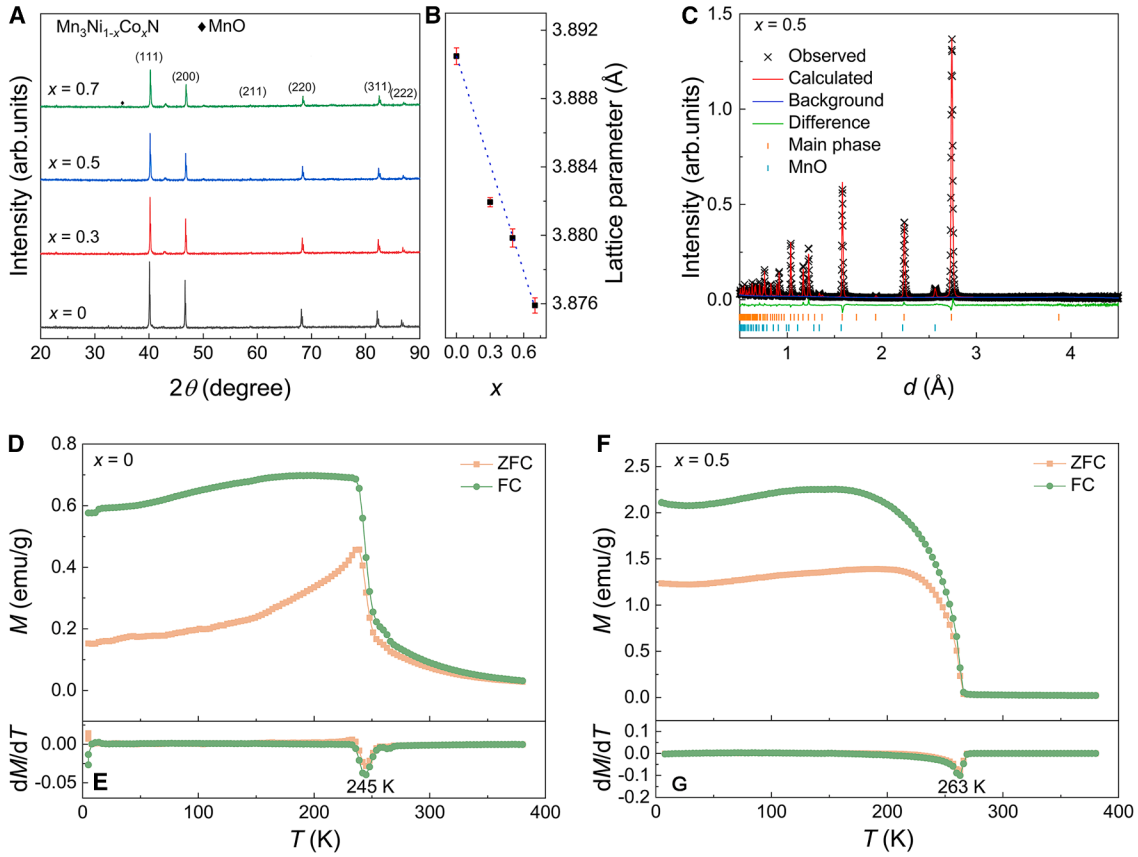

Figure 1. Crystal structure characterization and magnetic transition behavior of $Mn_3Ni_{1-x}Co_xN$ compounds

(A) Room temperature X-ray diffraction patterns for different Co concentrations (x = 0, 0.3, 0.5, 0.7).

(B) Lattice parameter variation as a function of Co content x, error bars represent the standard deviations obtained from Rietveld refinement.

(C) Rietveld refinement of the neutron diffraction pattern for the x = 0.5 sample. Temperature-dependent magnetization curves measured under zero-field-cooled (ZFC) and field-cooled (FC) conditions for (D) x = 0 and (F) x = 0.5. Temperature-dependent dM/dT derivative curves showing magnetic transition temperatures for (E) x = 0 and (G) x = 0.5.

microstructure through chemical doping or vacancy engineering represents the key strategy for tuning their physical properties.

Among the numerous Mn-based antiperovskite compounds, Mn_3NiN[28,29] has attracted considerable attention due to its unique magnetoelectric coupling characteristics. This compound exhibits rich magnetic structural changes within the magnetic ordering temperature range. At $T \leq 163$ K, the magnetic structure adopts a Γ^{5g} triangular AFM configuration, while for 163 K $\leq T \leq$ 266 K, it displays a coexistence of Γ^{4g} and Γ^{5g} AFM phases. In the AFM ordered state, Mn_3NiN shows metallic behavior with an increasing resistivity upon heating. More importantly, Mn_3NiN demonstrates significant NZ-TCR behavior,[12,30,31] showing potential for applications in precision resistor devices, electrical heating elements, and resistance measurement standards. However, its relatively low magnetic ordering temperature and limited magnetoelectric tuning range constrain further practical applications. Interestingly, the element Co is adjacent to Ni in the periodic table, and both are typical magnetic elements. Mn_3CoN has been reported to exhibit perpendicular magnetic anisotropy and substantial exchange bias effect.[19] These contrasting properties suggest that Co-Ni compositional tuning holds promise for effectively modulating magnetoelectric performance while maintaining structural stability. However, systematic and in-depth studies on how Co substitution affects the magnetic ordering evolution, phase transition behavior, and magnetoelectric transport mechanisms of Mn_3NiN remain lacking. Therefore, this work aims to systematically investigate the influence of Co substitution on the magnetic properties, thermal expansion, phase transition temperatures, and electronic transport behavior through the preparation of the $Mn_3Ni_{1-x}Co_xN$ compound series, thereby elucidating the regulatory mechanisms of Co substitution and providing fundamental insights for property modulation strategies in antiperovskite systems.

RESULTS AND DISCUSSION

Crystal structure and magnetic transition

Figure 1A presents the room temperature X-ray diffraction (XRD) patterns of $Mn_3Ni_{1-x}Co_xN$ (nominal x = 0, 0.3, 0.5, 0.7) samples. All samples are identified as having a cubic antiperovskite crystal structure with the space group $Pm\bar{3}m$ (No. 221), as confirmed by comparison with standard diffraction databases. While trace amounts of MnO impurity phase were detected, Rietveld

refinement reveals that its mass fraction remains below 5 wt % across all compositions, which has a negligible impact on the physical properties of the main $Mn_3Ni_{1-x}Co_xN$ phase. The cubic lattice parameter a decreases linearly with increasing Co content (Figure 1B), consistent with Vegard's law[32] and confirming successful Co substitution. Notably, this contraction occurs despite the similar atomic radii of Co and Ni (1.25 Å vs. 1.24 Å), reflecting the dominant role of MVEs over simple atomic size considerations in antiperovskite nitrides.[9] Neutron diffraction refinement of the sample with $x = 0.5$ at room temperature reveals that the actual composition is $Mn_3Ni_{0.45}Co_{0.55}N$, with an MnO impurity content of 2.51 wt %, as shown in Figure 1C. The detailed refinement parameters are provided in Table S1 of the supplemental information.

To further investigate the effect of Co doping at Ni sites on the magnetic properties of Mn_3NiN compounds, we measured the temperature dependence of magnetization of samples with $x = 0$ and $x = 0.5$ under both ZFC and FC conditions in the temperature range of 2–380 K using a Physical Property Measurement System (PPMS). As shown in Figure 1D, pristine Mn_3NiN ($x = 0$) exhibits characteristic AFM behavior upon cooling. We define the transition temperature using the $M(T)$ inflection identified by the extremum of dM/dT, yielding $T_t = 245$ K. Additionally, the $M(T)$ curve reaches a maximum of 0.69 emu g^{-1} at 236 K. The notably low magnetization values (<0.69 emu g^{-1}) further confirm the AFM nature of the undoped compound. This observation aligns with previous reports on antiperovskite manganese nitrides, where the Mn - Mn exchange interactions typically favor AFM coupling. In contrast, when the nominal Co doping content reaches 0.5, neutron diffraction refinement reveals that the actual composition is $Mn_3Ni_{0.45}Co_{0.55}N$. This Co-doped compound demonstrates distinctly different magnetic behavior (Figure 1F), exhibiting ferrimagnetic (FIM) characteristics with a significantly enhanced magnetization (approximately 3.26 times higher than the pristine sample Mn_3NiN). The transition from AFM to FIM ordering can be attributed to the modification of exchange interactions between Mn atoms mediated by Co substitution at Ni sites, which disrupts the AFM alignment of Mn moments and introduces competing magnetic interactions.

To precisely quantify the magnetic transition temperatures in both compounds, we conducted derivative analysis on the magnetization curves. The resulting dM/dT versus temperature plots, presented in Figures 1E and 1G, provide a more accurate determination of the critical transition temperatures. These derivative curves clearly demonstrate that Co doping not only transforms the magnetic ordering but also elevates the magnetic transition temperature from 245 K ($x = 0$) to 263 K ($x = 0.5$). This 18 K increase in transition temperature, coupled with the substantial magnetization enhancement, underscores the significant impact of Co substitution on the magnetic exchange network within the antiperovskite structure. Such modifications to the magnetic properties through controlled chemical substitution offer promising pathways for tailoring these materials for specific technological applications.

Exchange bias effect

Based on the above analysis of temperature-dependent magnetization, we found that Co doping leads to significant changes in the magnetic ordering state. To further elucidate the specific effects of these magnetic ordering changes on magnetic behavior, we measured the isothermal magnetization curves of samples with $x = 0$ and $x = 0.5$ at 25 K, 75 K, 150 K, 200 K, and 300 K (see Figures 2A–2E). For the sample with $x = 0$, the $M(H)$ curves exhibit nearly linear behavior with minimal hysteresis, consistent with its predominantly AFM nature. In contrast, when the Co content is $x = 0.5$, the sample displays pronounced hysteresis loops in the magnetically ordered phase (below 263 K), indicating the emergence of significant FM components within the system. Notably, the magnetization of the Co-doped sample does not reach saturation even at high fields, suggesting the persistence of some AFM interactions alongside the FM ordering. This coexistence of AFM and FM contributions, combined with the enhanced net magnetization observed in the $M(T)$ curves, collectively supports our conclusion that Co doping transforms the magnetic structure from AFM to FIM state, where magnetic moments align in an uncompensated antiparallel arrangement.

Particularly noteworthy is that the $M(H)$ curves of $x = 0.5$ exhibit pronounced asymmetric hysteresis loops at different temperatures, especially at 25 K and 75 K, where the loops shift toward the negative magnetic field direction. This behavior contrasts sharply with the symmetric response of the AFM parent compound Mn_3NiN. Co-doping introduces ferromagnetic components, and the exchange coupling between FM and AFM phases results in the asymmetric hysteresis loops, namely the exchange bias effect. As temperature increases to 150 K, the shift of the hysteresis loops in the $x = 0.5$ sample gradually disappears. According to the $M(T)$ curves, the $x = 0.5$ sample enters a magnetic transition region above 150 K, where the system undergoes a gradual transition from the magnetically ordered state toward the paramagnetic state, characterized by weakening magnetism and diminishing exchange coupling between FM and AFM phases.

The exchange bias field is defined as $H_{EB} = |H_L + H_R|/2$, and the coercivity is defined as $H_C = |H_L - H_R|/2$, where H_L and H_R are the coercive fields on the negative and positive magnetic field axes, respectively. We calculated the exchange bias field and coercivity for the samples with $x = 0$ and $x = 0.5$ at different temperatures, as shown in Table S2. Figure 2F demonstrates that after Co doping, the compound exhibits significant exchange bias phenomena in the low-temperature magnetically ordered region. The exchange bias field for the $x = 0.5$ sample reaches a maximum of approximately 7.44 kOe at $T = 25$ K and gradually decreases with increasing temperature, approaching zero at $T \geq 150$ K. The coercivity shows a trend of first increasing and then decreasing with temperature, reaching a maximum of approximately 9.45 kOe at $T = 75$ K. At 300 K, the $x = 0.5$ sample is in the paramagnetic state, consistent with the coercivity approaching zero.

Generally, shape anisotropy, magnetoelastic anisotropy, and magnetocrystalline anisotropy are the primary sources of coercivity in magnetic materials.[33] Although Mn-based antiperovskites possess a cubic crystal structure and exhibit isotropic thermal expansion behavior, local structural distortions or magnetic sublattice ordering may introduce significant magnetocrystalline anisotropy. We believe this anisotropy is the dominant factor responsible for the large coercivity in the $x = 0.5$ sample. Furthermore, the disappearance of the exchange bias field and

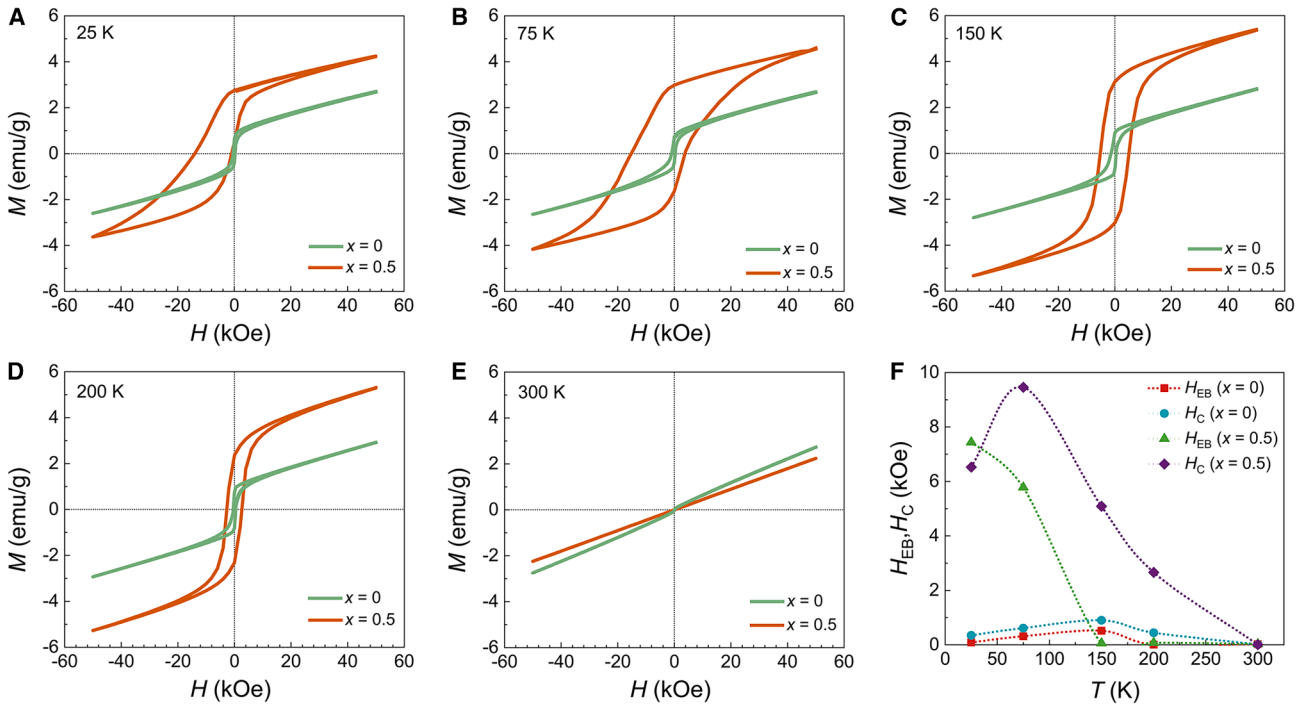

Figure 2. Temperature-dependent magnetic hysteresis loops and exchange bias properties

(A–E) Isothermal magnetization curves for samples with $x = 0$ and $x = 0.5$ measured at 25 K, 75 K, 150 K, 200 K, and 300 K, respectively.

(F) Temperature dependence of exchange bias field (H_{EB}) and coercivity (H_C) for $x = 0$ and $x = 0.5$ compounds.

the reduction in coercivity correspond precisely to the onset of magnetization decrease at 150 K in the $M(T)$ curves, indicating the gradual entry into the magnetic transition regime. Such materials exhibiting exchange bias phenomena have broad application prospects in spin valve devices, ultra-high-density magnetic recording media, and other fields.

Electronic and magnetic transport behaviors

Mn_3NiN is a typical antiperovskite compound exhibiting a near-zero temperature coefficient of resistivity. To investigate the influence of magnetic Co doping on its electronic and magnetic transport behaviors, we measured the normalized resistivity of $Mn_3Ni_{1-x}Co_xN$ ($x = 0, 0.3, 0.5, 0.7$) compounds and characterized the AHE behavior for the $x = 0.5$ sample. Figure 3A shows the temperature dependence of normalized electronic resistivity ($\Delta\rho/\rho_{300\ K}$) for $Mn_3Ni_{1-x}Co_xN$ compounds measured from 10 K to 350 K. All samples maintain similar metallic transport behavior to Mn_3NiN below the transition temperature, demonstrating a linear increase in resistivity due to dominant electron-phonon scattering in the metallic regime, followed by an NZ-TCR behavior above the transition temperature. Previous studies have indicated that this nearly temperature-independent resistivity behavior in the paramagnetic state is closely correlated with spin-disorder scattering.[12] Quantitative analysis of the temperature coefficient of resistivity, calculated using $\rho_0^{-1}d\rho/dT$[34] in the high temperature regime above each transition temperature (Figure S1), reveals the following values: -1.36×10^{-5} K^{-1} ($x = 0$, 265 K–350 K), -4.24×10^{-4} K^{-1} ($x = 0.3$, 263 K–350 K), 3.87×10^{-5} K^{-1} ($x = 0.5$, 260 K–350 K), and -4.39×10^{-5} K^{-1} ($x = 0.7$, 275 K–350 K). The variation in TCR values with Co substitution suggests a systematic modulation of the electronic transport properties, potentially reflecting changes in the magnetic exchange interactions and electronic band structure upon Co doping.

Furthermore, to gain deeper insights into the electronic transport properties, we performed AHE measurements and analysis on the $x = 0.5$ sample. It is well established that the total transverse resistivity measured under various magnetic fields comprises both the ordinary and anomalous Hall contributions,[35] as described by Equation 1:

$$\rho_{xy} = \rho_{xy}^0 + \rho_{xy}^A \quad \text{(Equation 1)}$$

Of which the ordinary Hall resistivity can be expressed as ρ_{xy}^0:

$$\rho_{xy}^0 = R_0\mu_0 H \quad \text{(Equation 2)}$$

The ordinary Hall resistivity arises from the deflection of charge carriers under the Lorentz force as they move in a perpendicular magnetic field. In addition to the ordinary Hall resistivity, we denote the anomalous Hall resistivity as ρ_{xy}^A. To extract the anomalous Hall component from the experimental data, we first correct for the ordinary Hall effect by calculating the slope α of the ρ_{xy} curves at high magnetic fields on both ends and taking their average. The ordinary Hall resistivity is then given by $\rho_{xy}^0 = \overline{\alpha}H$. Subtracting this ordinary contribution from the total Hall resistivity ρ_{xy} yields the anomalous Hall resistivity ρ_{xy}^A.

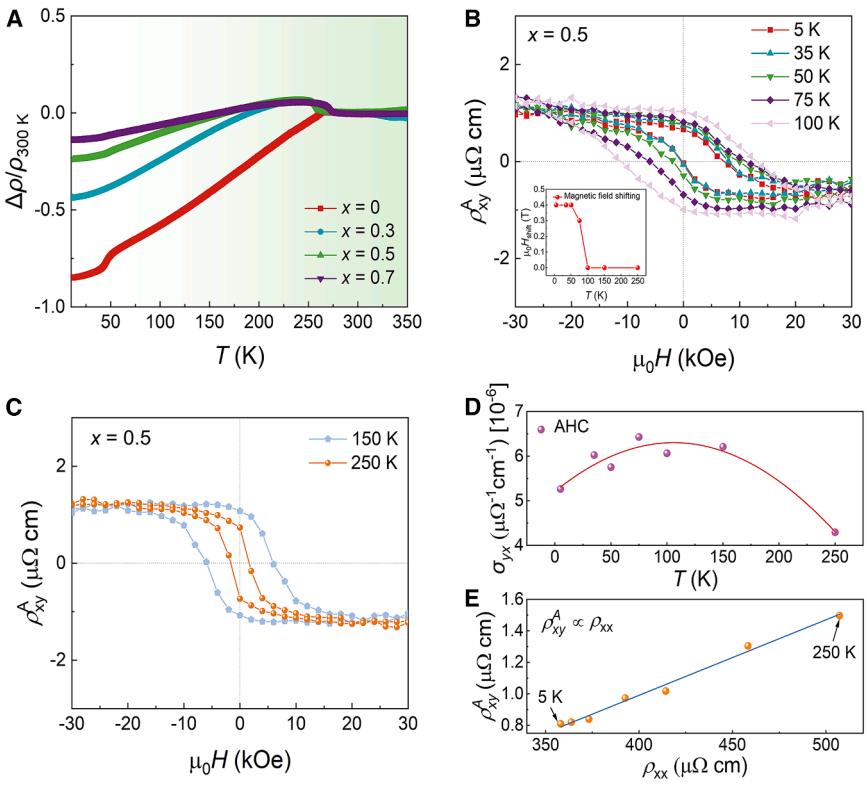

Figure 3. Electronic transport properties and anomalous Hall effect in $Mn_3Ni_{1-x}Co_xN$ compounds

(A) Normalized resistivity of $Mn_3Ni_{1-x}Co_xN$ (x = 0, 0.3, 0.5, 0.7) compounds as a function of temperature.

(B and C) Magnetic field dependence of the anomalous Hall resistivity of the x = 0.5 sample at various temperatures. The inset in (B) shows the temperature dependence of the anomalous Hall offset under an applied magnetic field.

(D) Temperature dependence of the anomalous Hall conductivity (AHC) of the x = 0.5 sample, with the red solid line representing the fitting curve.

(E) Scaling relationship between anomalous Hall resistivity (ρ^A_{xy}) and longitudinal resistivity (ρ_{xx}) over the temperature range of 5–250 K, with the blue line showing the linear fit and demonstrating the intrinsic nature of the anomalous Hall effect.

As shown in Figures 3B and 3C, the Co-doped compound (x = 0.5) exhibits a pronounced AHE over the temperature range of 5–250 K. The introduction of Co induces a ferromagnetic component, which further favors the emergence of the AHE. Interestingly, in the temperature range from 5 K to 75 K, the measured AHE curves exhibit a systematic offset under applied magnetic fields, as illustrated in the inset of Figure 3B. With increasing temperature, this shift gradually diminishes and disappears around 100 K. In conjunction with the magnetic susceptibility $M(T)$ and isothermal magnetization $M(H)$ results, we attribute this behavior to the coexistence of ferromagnetic and AFM exchange coupling, which gives rise to an exchange bias effect in the Co-doped compound at low temperatures. This exchange bias effect is responsible for the observed field-dependent behavior of the AHE.

Meanwhile, we calculated the temperature dependence of the AHC for the x = 0.5 compound and performed a fitting analysis, as shown in Figure 3D. The results indicate that the AHC of x = 0.5 first increases and then decreases within the temperature range of 5–250 K. It reaches a maximum value of $6.43 \times 10^{-6}\ \mu\Omega^{-1}cm^{-1}$ at 75 K and gradually decreases to its minimum at 250 K. The observed trend in AHC reflects, to some extent, the magnetic evolution of the compound. In addition, we analyzed the relationship between the anomalous Hall resistivity (ρ^A_{xy}) and the longitudinal resistivity (ρ_{xx}),[36] as presented in Figure 3E. The fitting results show that $\rho^A_{xy} = 0.00479\rho_{xx}$, indicating a linear correlation between ρ^A_{xy} and ρ_{xx}. This suggests that the skew scattering mechanism predominantly contributes to the AHE in the magnetically ordered state.[37]

Thermal expansion and phase transition characteristics

Given that Co substitution introduces ferromagnetic components into the $Mn_3Ni_{1-x}Co_xN$ system, and previous studies[6,11,38] have demonstrated that thermal expansion is intimately correlated with magnetic phase transitions in antiperovskite materials, we further investigated the thermal expansion behavior to elucidate the coupling effects. As shown in Figure 4A, the thermal expansion behavior of the $Mn_3Ni_{1-x}Co_xN$ (x = 0, 0.3, 0.5, 0.7) series of compounds was measured using a DIL 402C dilatometer over the temperature range of 123 K–473 K, with L_0 representing the sample length at 123 K. By analyzing the thermal expansion curves within the temperature range corresponding to the anomalous thermal expansion response, the CTE of the samples were obtained, as summarized in Table S3. As a typical AFM material, the antiperovskite nitride Mn_3NiN exhibits a sharp volume contraction near the magnetic transition temperature, known as the MVE, resulting in a pronounced negative thermal expansion behavior. Figure 4A reveals that substituting Co for Ni in the cubic Mn_3NiN structure has a significant impact on its anomalous thermal expansion behavior. With increasing Co content, the transition temperature of the anomalous thermal expansion in the $Mn_3Ni_{1-x}Co_xN$ series decreases from 273 K (x = 0) to 267 K (x = 0.3), and then increases with further Co substitution, reaching 271 K at x = 0.5 and 272 K at x = 0.7. Meanwhile, the CTE shows a trend of first decreasing and then increasing, from $-65.64 \times 10^{-6}\ K^{-1}$ (x = 0) to $-76.28 \times 10^{-6}\ K^{-1}$ (x = 0.3), and subsequently increasing to $-23.55 \times 10^{-6}\ K^{-1}$ (x = 0.7). These thermal expansion results indicate that, due to the similar positions of Co and Ni in the elemental periodic table, a small amount of Co doping has minimal effect on the thermal expansion behavior of Mn_3NiN. However, at higher of Co substitution levels, the anomalous thermal expansion behavior is gradually suppressed. This phenomenon is attributed to the introduction of partial ferromagnetic components by Co doping, which

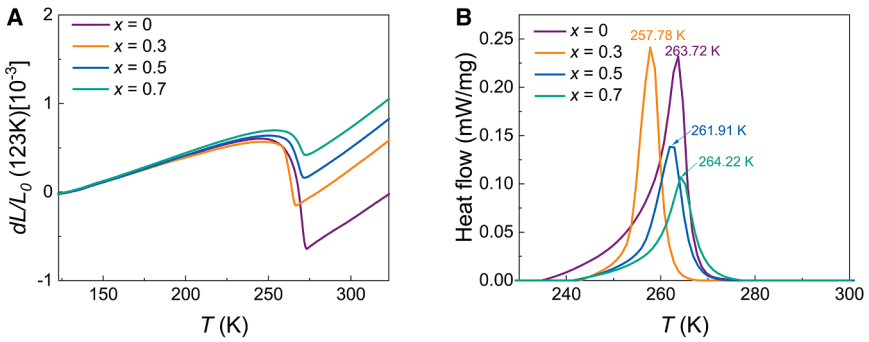

Figure 4. Thermal properties of $Mn_3Ni_{1-x}Co_xN$ compounds

(A) Thermal expansion behaviors of $Mn_3Ni_{1-x}Co_xN$ (x = 0, 0.3, 0.5, 0.7) compounds.

(B) DSC heat flow curves for $Mn_3Ni_{1-x}Co_xN$ compounds.

suppresses the MVE in the system, thereby weakening the negative thermal expansion change.

To further confirm the variation in the phase transition temperatures of the $Mn_3Ni_{1-x}Co_xN$ series of compounds, DSC measurements were performed to obtain the heat flow curves for the samples with x = 0, 0.3, 0.5, and 0.7. Since the magnetic order-disorder transition (upon heating) in Mn-based antiperovskite compounds is an endothermic process and classified as a first-order phase transition, DSC can be used to quantitatively characterize the thermal effects in these compounds and accurately determine their phase transition temperatures. As illustrated in Figure 4B, the phase transition temperature in the $Mn_3Ni_{1-x}Co_xN$ series exhibits a non-monotonic dependence on Co substitution content, initially decreasing and subsequently increasing with higher Co concentrations. This behavior is consistent with the trends observed in both the thermal expansion measurements and the TCR transition temperatures. Specifically, the phase transition temperature decreases from 263.72 K (x = 0) to 257.78 K (x = 0.3), and then increases to 261.91 K (x = 0.5) and 264.22 K (x = 0.7) as the Co content increases further. According to the $M(T)$ curve of the x = 0.5 sample, the phase transition temperature determined by DSC is consistent with the magnetic measurement results, and also matches the negative thermal expansion temperature range, indicating that these compounds exhibit strong "spin-lattice-charge" coupling.

By partially substituting the corner-site Ni atoms in the cubic lattice of Mn_3NiN with a certain amount of magnetic Co atoms, we systematically investigated the lattice, magnetic properties, thermal expansion behaviors, phase transition temperatures, and electronic transport behaviors of the $Mn_3Ni_{1-x}Co_xN$ series of compounds. Co-doping introduces a ferromagnetic component, enabling the coexistence of AFM and FM phases in $Mn_3Ni_{1-x}Co_xN$. Notably, the x = 0.5 sample exhibits a pronounced exchange bias effect at low temperatures, with a maximum exchange bias field of 7.44 kOe at T = 25 K. The coercivity reaches a maximum of approximately 9.45 kOe at T = 75 K. Moreover, Co doping significantly modulates the electronic transport properties, and a remarkable AHE was observed in the magnetically ordered region. Further analysis reveals that the AHE is primarily governed by the skew scattering mechanism. Overall, the $Mn_3Ni_{1-x}Co_xN$ series demonstrates rich magnetic tunability and unconventional magnetotransport characteristics, providing an experimental foundation and theoretical insights for the design and application of Mn-based antiperovskite magnetic materials.

Limitations of the study

This study focused on magnetic element substitution (Ni-Co) and its effects on magnetic properties. However, investigations of magnetic-to-nonmagnetic element substitutions and the role of nonmagnetic elements in antiperovskite materials remain limited, which could contribute to a more comprehensive understanding of magnetic transition behaviors in this material family.

RESOURCE AVAILABILITY

Lead contact

Requests for further information and resources should be directed to and will be fulfilled by the lead contact, Cong Wang (congwang@buaa.edu.cn).

Materials availability

All unique reagents generated in this study are available from the lead contact with a completed materials transfer agreement.

Data and code availability

- All data reported in this paper will be shared by the lead contact upon request.
- This paper does not report original code.
- Any additional information required to reanalyze the data reported in this paper is available from the lead contact upon request.

ACKNOWLEDGMENTS

We thank the staff members of the high-pressure neutron diffractometer (https://cstr.cn/31113.02.CSNS.HPND) at the China Spallation Neutron Source (CSNS) (https://cstr.cn/31113.02.CSNS), for providing technical support and assistance in data collection and analysis.

This research was financially supported by the National Key R&D Program of China (No. 2022YFA1402604 and 2021YFA1600603), the Guangdong Basic and Applied Basic Research Foundation (2025B1515020087), the National Natural Science Foundation of China (nos. 52272264, 52371190, and 92366301), the Ye Minghan Public Welfare Development Project (X21520608), and the Large Scientific Facility Open Subject of Songshan Lake (KFKT2022B07), Dongguan.

AUTHOR CONTRIBUTIONS

C.W. and D.H. designed this study. D.H. was responsible for the material preparation and characterizations. Y.S. and K.S. analyzed and interpreted the XRD results. C.S. and D.H. collected and analyzed electronic and magnetic transport data. G.F. performed the magnetic measurements and contributed to the interpretation of the magnetic results. X.S., D.G., and Z.L. conducted

neutron powder diffraction experiments. B.Y., L.K., and S.D. analyzed and interpreted the neutron diffraction data. D.H., S.D., and L.K. drafted the manuscript. All authors contributed to data interpretation, critically revised the manuscript, and approved the final version for submission.

DECLARATION OF INTERESTS

The authors declare no competing interests.

STAR★METHODS

Detailed methods are provided in the online version of this paper and include the following:

- KEY RESOURCES TABLE
- METHOD DETAILS
  - Sample preparation
  - Structural characterization
  - Magnetic and transport measurements
  - Thermal analysis
- QUANTIFICATION AND STATISTICAL ANALYSIS

SUPPLEMENTAL INFORMATION

Supplemental information can be found online at https://doi.org/10.1016/j.isci.2026.115300.

Received: September 25, 2025
Revised: December 16, 2025
Accepted: March 5, 2026
Published: March 10, 2026

REFERENCES

1. Hua, L., Wang, L., Chen, L.F., Wang, L., and Chen, L.F. (2010). First-principles investigation of Ge doping effects on the structural, electronic and magnetic properties in antiperovskite Mn_3CuN. J. Phys. Condens. Matter *22*, 206003. https://doi.org/10.1088/0953-8984/22/20/206003.
2. Mochizuki, M., Kobayashi, M., Okabe, R., and Yamamoto, D. (2018). Spin model for nontrivial types of magnetic order in inverse-perovskite antiferromagnets. Phys. Rev. B *97*, 060401. https://doi.org/10.1103/PhysRevB.97.060401.
3. Shen, Q., van Dijk, N., Brück, E., and Li, L. (2025). Exploring Zero Thermal Expansion in Magnetocaloric Materials. Adv. Eng. Mater. *27*, 2500833. https://doi.org/10.1002/adem.202500833.
4. Shen, Q., van Rooij, F., Zhang, Z., Hao, W., Dugulan, A.I., van Dijk, N., Brück, E., and Li, L. (2026). Tunable magnetoelastic transition and enhanced magnetocaloric response in $Hf_{0.82}Ta_{0.18}Fe_2$ Laves phase alloys by Fe (6*h*)-site manipulation. J. Mater. Sci. Technol. *254*, 196–205. https://doi.org/10.1016/j.jmst.2025.08.015.
5. Wang, H., Xu, Y., Song, Y., Sanson, A., Zhang, Y., Yao, Y., Liu, H., Watanabe, T., Zeng, J., Shi, N., and Chen, J. (2025). Isotropic Zero Thermal Expansion in $Yb(Al,Mn)_2$: Achieving Continuous Shiftability over a Wide Temperature Range. J. Am. Chem. Soc. *147*, 34697–34705. https://doi.org/10.1021/jacs.5c10024.
6. Shi, K., Sun, Y., Colin, C.V., Wang, L., Yan, J., Deng, S., Lu, H., Zhao, W., Kazunari, Y., Bordet, P., and Wang, C. (2018). Investigation of the spin-lattice coupling in $Mn_3Ga_{1-x}Sn_xN$ antiperovskites. Phys. Rev. B *97*, 054110. https://doi.org/10.1103/PhysRevB.97.054110.
7. Hu, D., Shi, K., Sun, Y., Colin, C.V., Deng, S., An, S., Ma, Z., Bordet, P., and Wang, C. (2025). Effect of Fe-doping on magnetic structures and "spin-lattice-charge" strong correlation properties in $Mn_3Sn_{1-x}Fe_xC$ compounds. J. Alloys Compd. *1010*, 177489. https://doi.org/10.1016/j.jallcom.2024.177489.
8. Hamada, T., and Takenaka, K. (2012). Phase instability of magnetic ground state in antiperovskite Mn_3ZnN: Giant magnetovolume effects related to magnetic structure. J. Appl. Phys. *111*, 07A904. https://doi.org/10.1063/1.3670052.
9. Takenaka, K., Ichigo, M., Hamada, T., Ozawa, A., Shibayama, T., Inagaki, T., and Asano, K. (2014). Magnetovolume effects in manganese nitrides with antiperovskite structure. Sci. Technol. Adv. Mater. *15*, 015009. https://doi.org/10.1088/1468-6996/15/1/015009.
10. Lin, J.C., Tong, P., Tong, W., Lin, S., Wang, B.S., Song, W.H., Zou, Y.M., and Sun, Y.P. (2015). Tunable negative thermal expansion related with the gradual evolution of antiferromagnetic ordering in antiperovskite manganese nitrides $Ag_{1-x}NMn_{3+x}$ ($0 \leq x \leq 0.6$). Appl. Phys. Lett. *106*, 082405. https://doi.org/10.1063/1.4913663.
11. Wang, C., Chu, L., Yao, Q., Sun, Y., Wu, M., Ding, L., Yan, J., Na, Y., Tang, W., Li, G., et al. (2012). Tuning the range, magnitude, and sign of the thermal expansion in intermetallic $Mn_3(Zn, M)_xN$(M = Ag, Ge). Phys. Rev. B *85*, 220103. https://doi.org/10.1103/PhysRevB.85.220103.
12. Ding, L., Wang, C., Chu, L., Yan, J., Na, Y., Huang, Q., and Chen, X. (2011). Near zero temperature coefficient of resistivity in antiperovskite $Mn_3Ni_{1-x}Cu_xN$. Appl. Phys. Lett. *99*, 251905. https://doi.org/10.1063/1.3671183.
13. Kamishima, K., Goto, T., Nakagawa, H., Miura, N., Ohashi, M., Mori, N., Sasaki, T., and Kanomata, T. (2000). Giant magnetoresistance in the intermetallic compound Mn_3GaC. Phys. Rev. B *63*, 024426. https://doi.org/10.1103/PhysRevB.63.024426.
14. Yan, J., Sun, Y., Wen, Y., Chu, L., Wu, M., Huang, Q., Wang, C., Lynn, J.W., and Chen, Y. (2014). Relationship between spin ordering, entropy, and anomalous lattice variation in $Mn_3Sn_{1-\varepsilon}Si_\varepsilon C_{1-\delta}$ compounds. Inorg. Chem. *53*, 2317–2324. https://doi.org/10.1021/ic403063t.
15. Yan, J., Sun, Y., Wu, H., Huang, Q., Wang, C., Shi, Z., Deng, S., Shi, K., Lu, H., and Chu, L. (2014). Phase transitions and magnetocaloric effect in $Mn_3Cu_{0.89}N_{0.96}$. Acta Mate *74*, 58–65. https://doi.org/10.1016/j.actamat.2014.04.005.
16. Lin, J.C., Wang, B.S., Lin, S., Tong, P., Lu, W.J., Zhang, L., Zhao, B.C., Song, W.H., and Sun, Y.P. (2012). The study of structure, magnetism, electricity, and their correlations at martensitic transition for magnetostriction system $Cu_{1-x}Mn_xNMn_3$ ($0 \leq x \leq 0.5$). J. Appl. Phys. *111*, 113914. https://doi.org/10.1063/1.4725471.
17. Asano, K., Koyama, K., and Takenaka, K. (2008). Magnetostriction in Mn_3CuN. Appl. Phys. Lett. *92*, 161909. https://doi.org/10.1063/1.2917472.
18. Lin, J.C., Tong, P., Cui, D.P., Yang, C., Lin, S., Lu, W.J., Wang, B.S., Zhao, B.C., and Sun, Y.P. (2015). Exchange bias induced after zero-field cooling in antiperovskite compounds $Ga_{1-x}NMn_{3+x}$. Phys. Status Solidi *252*, 582–588. https://doi.org/10.1002/pssb.201451389.
19. Sun, Y., Hu, P., Shi, K., Wu, H., Deng, S., Huang, Q., Mao, Z., Song, P., Wang, L., Hao, W., et al. (2019). Giant zero-field cooling exchange-bias-like behavior in antiperovskite $Mn_3Co_{0.61}Mn_{0.39}N$ compound. Phys. Rev. Mater. *3*, 024409. https://doi.org/10.1103/PhysRevMaterials.3.024409.
20. Zhao, K., Hajiri, T., Chen, H., Miki, R., Asano, H., and Gegenwart, P. (2019). Anomalous Hall effect in the noncollinear antiferromagnetic antiperovskite $Mn_3Ni_{1-x}Cu_xN$. Phys. Rev. B *100*, 045109. https://doi.org/10.1103/PhysRevB.100.045109.
21. Huyen, V.T.N., Suzuki, M.T., Yamauchi, K., and Oguchi, T. (2019). Topology analysis for anomalous Hall effect in the noncollinear antiferromagnetic states of Mn_3AN (A = Ni, Cu, Zn, Ga, Ge, Pd, In, Sn, Ir, Pt). Phys. Rev. B *100*, 094426. https://doi.org/10.1103/PhysRevB.100.094426.
22. Kobayashi, M., and Mochizuki, M. (2019). Theory of magnetism-driven negative thermal expansion in inverse perovskite antiferromagnets. Phys. Rev. Mater. *3*, 024407. https://doi.org/10.1103/PhysRevMaterials.3.024407.
23. An, S., Yang, F., Sun, Y., Deng, S., Yuan, X., Shi, K., He, L., Yuan, B., Sun, L., Guo, J., et al. (2025). Emergent Multiple Spin States From

Baromagnetic Effect in Strongly Correlated Magnet Mn_3GaC. Adv. Mater. *37*, e2420502. https://doi.org/10.1002/adma.202420502.

24. Ma, Z., Sun, Y., Lu, H., Shi, K., Deng, S., Yuan, X., Hao, W., Du, Y., Xia, Y., Fang, L., et al. (2023). Noncoplanar antiferromagnetism induced zero thermal expansion behavior in the antiperovskite $Mn_3Sn_{0.5}Zn_{0.5}C_x$. Phys. Rev. B *107*, 094412. https://doi.org/10.1103/PhysRevB.107.094412.
25. Takenaka, K., Ozawa, A., Shibayama, T., Kaneko, N., Oe, T., and Urano, C. (2011). Extremely low temperature coefficient of resistance in antiperovskite $Mn_3Ag_{1-x}Cu_xN$. Appl. Phys. Lett. *98*, 022103. https://doi.org/10.1063/1.3541449.
26. Hadano, M., Ozawa, A., Takenaka, K., Kaneko, N., Oe, T., and Urano, C. (2012). Interplay between magnetism and charge transport in antiperovskite manganese nitrides: Extremely low temperature coefficient of resistance due to strong magnetic scattering. J. Appl. Phys. *111*, 07e120. https://doi.org/10.1063/1.3673425.
27. Lin, J.C., Tong, P., Lin, S., Wang, B.S., Song, W.H., and Sun, Y.P. (2014). Continuously tunable temperature coefficient of resistivity in antiperovskite $AgN_{1-x}C_xMn_3$ ($0 \leq x \leq 0.15$). J. Appl. Phys. *116*, 213912. https://doi.org/10.1063/1.4903699.
28. Wu, M., Wang, C., Sun, Y., Chu, L., Yan, J., Chen, D., Huang, Q., and Lynn, J.W. (2013). Magnetic structure and lattice contraction in Mn_3NiN. J. Appl. Phys. *114*, 123902. https://doi.org/10.1063/1.4822023.
29. Fruchart, D., and F Bertaut, E. (1978). Magnetic Studies of the Metallic Perovskite-Type Compounds of Manganese. J. Phys. Soc. Jpn. *44*, 781–791. https://doi.org/10.1143/JPSJ.44.781.
30. Deng, S., Sun, Y., Wang, L., Wu, H., Shi, K., Hu, P., Huang, Q., and Wang, C. (2016). Near-zero temperature coefficient of resistivity associated with magnetic ordering in antiperovskite $Mn_{3+x}Ni_{1-x}N$. Appl. Phys. Lett. *108*, 041908. https://doi.org/10.1063/1.4940912.
31. Sun, Y., Wang, C., Chu, L., Wen, Y., Nie, M., and Liu, F. (2010). Low temperature coefficient of resistivity induced by magnetic transition and lattice contraction in Mn_3NiN compound. Scr. Mater. *62*, 686–689. https://doi.org/10.1016/j.scriptamat.2010.01.027.
32. Denton, A.R., and Ashcroft, N.W. (1991). Vegard's law. Phys. Rev. A *43*, 3161–3164. https://doi.org/10.1103/PhysRevA.43.3161.
33. Zhang, H.-w., Zhao, T.-y., Zhang, J., Rong, C.-b., Zhang, S.-y., Shen, B.-g., Li, L., and Zhang, L.-g. (2003). Large coercivity in nanocrystalline TbMn6Sn6 permanent magnets prepared by mechanical milling. J. Phys. D Appl. Phys. *36*, 1769–1772. https://doi.org/10.1088/0022-3727/36/15/303.
34. Wang, J., Shi, K., Sun, Y., Deng, S., Zhang, K., Cui, J., Hu, D., Zhao, W., and Wang, C. (2024). A new noncollinear triangle antiferromagnetic phase in Mn_3GaN by Cr doping. Mater. Today Phys. *42*, 101362. https://doi.org/10.1016/j.mtphys.2024.101362.
35. Pugh, E.M., and Rostoker, N. (1953). Hall effect in ferromagnetic materials. Rev. Mod. Phys. *25*, 151–157. https://doi.org/10.1103/RevModPhys.25.151.
36. Tian, Y., Ye, L., and Jin, X. (2009). Proper scaling of the anomalous Hall effect. Phys. Rev. Lett. *103*, 087206. https://doi.org/10.1103/PhysRevLett.103.087206.
37. Han, H., Sun, Y., Shi, K., Yuan, X., Ren, J., Cui, J., Hu, D., Zhang, K., and Wang, C. (2022). Sign reversal of the anomalous Hall effect in antiperovskite (110)-oriented $Mn_{3.19}Ga_{0.81}N_{1-\delta}$ film. J. Appl. Phys. *132*, 233902. https://doi.org/10.1063/5.0105925.
38. Deng, S., Sun, Y., Wu, H., Huang, Q., Yan, J., Shi, K., Malik, M.I., Lu, H., Wang, L., Huang, R., et al. (2015). Invar-like Behavior of Antiperovskite $Mn_{3+x}Ni_{1-x}N$ Compounds. Chem. Mater. *27*, 2495–2501. https://doi.org/10.1021/cm504702m.
39. Rietveld, H.M. (1969). A profile refinement method for nuclear and magnetic structures. J. Appl. Cryst. *2*, 65–71. https://doi.org/10.1107/S0021889869006558.
40. Rodríguez-Carvajal, J. (1993). Recent advances in magnetic structure determination by neutron powder diffraction. Physica B *192*, 55–69. https://doi.org/10.1016/0921-4526(93)90108-I.

STAR★METHODS

KEY RESOURCES TABLE

REAGENT or RESOURCE	SOURCE	IDENTIFIER
Chemicals, peptides, and recombinant proteins		
Mn powder	Innochem	99.99% purity
Ni powder	Alfa Aesar	99.8% purity
Co powder	Innochem	99.9% purity
N_2 gas	Beijing Huanyu Jinghui Jingcheng Gas Technology Co., Ltd.	99.999% purity
Software and algorithms		
GSAS-II	Argonne National Laboratory	https://gsas-ii.readthedocs.io
NETZSCH Proteus	NETZSCH	https://analyzing-testing.netzsch.com/en/products/software/proteus
Other		
Bruker D8 Advance diffractometer	Bruker	D8 Advance
High Pressure Neutron Diffractometer (HPND)	China Spallation Neutron Source	HPND
Physical Property Measurement System (PPMS)	Quantum Design	Dynacool-14
Magnetic Property Measurement System (MPMS)	Quantum Design	Quantum Design MPMS3
Netzsch DIL 402C dilatometer	Netzsch	DIL 402C
NETZSCH DSC 200 F3 Maia	Netzsch	DSC 200 F3 Maia

METHOD DETAILS

Sample preparation

Polycrystalline $Mn_3Ni_{1-x}Co_xN$ ($x = 0, 0.3, 0.5, 0.7$) samples were synthesized by a vacuum solid-state sintering method. First, Mn powder was placed in an alumina boat and annealed at 1023 K for 48 h under a N_2 atmosphere to obtain an Mn_2N precursor powder. The as-prepared Mn_2N, together with stoichiometric amounts of Ni and Co powders, was thoroughly mixed in an agate mortar. The homogenized mixture was then pressed into pellets using a tablet press, wrapped in tantalum foil, and vacuum-sealed in quartz tubes (at a vacuum pressure below 10^{-2} Pa). Finally, the sealed samples were sintered at 1073 K for 80 h in a muffle furnace, followed by cooling to room temperature to obtain the desired polycrystalline samples.

Structural characterization

To determine the crystal structure and phase purity of $Mn_3Ni_{1-x}Co_xN$ samples, room temperature X-ray diffraction (XRD) patterns were collected using a Bruker D8 Advance diffractometer with Cu Kα radiation.

Neutron powder diffraction (NPD) measurements were performed on $Mn_3Ni_{1-x}Co_xN$ (nominal $x = 0.5$) at room temperature using the High-Pressure Neutron Diffractometer (HPND) at the China Spallation Neutron Source (CSNS) in time-of-flight (TOF) mode. During NPD measurements, samples were loaded into VNi null-matrix cans with a diameter of 6 mm. Data were collected over a neutron wavelength range of 0.71–5.8 Å. The VNi null-matrix cans were used to protect the samples from atmospheric moisture while minimizing background contributions to the NPD data. The structural parameters were refined through Rietveld analysis[39] using the GSAS-II[40] software. The refinement quality was evaluated primarily by the weighted-profile R factor (R_{wp}) and the goodness-of-fit (GOF).

Magnetic and transport measurements

Magnetic properties were characterized using a Physical Property Measurement System (PPMS) and Magnetic Property Measurement System (MPMS). Temperature-dependent magnetization measurements were performed in the range of 2–380 K under a magnetic field of 500 Oe using both zero-field-cooled (ZFC) and field-cooled (FC) protocols, and isothermal magnetization curves were recorded under magnetic fields up to ±5 kOe. In addition, the AHE at various temperatures was also measured using the PPMS. Resistivity (ρ) was measured using a standard four-probe technique in the temperature range of 10–350 K. A bulk specimen with dimensions of approximately $3 \times 1 \times 1$ mm^3 was contacted with copper wires using silver epoxy. The resistance was measured using a constant-current method with an excitation current of 100 mA, and ρ was calculated from the measured resistance and sample geometry.

Thermal analysis

Thermal expansion ($\Delta L/L_0$) of a bulk specimen ($\sim 10 \times 5 \times 5$ mm^3) was measured using a dilatometer (Netzsch DIL 402C) under a flowing He atmosphere, after cooling with liquid nitrogen, on heating at 5 K min^{-1} from 123 to 473 K.

Differential scanning calorimetry (DSC) was performed using a NETZSCH DSC 200 F3 Maia to record heat-flow curves under a flowing N_2 atmosphere. The measurements were carried out on heating at a rate of 10 K min^{-1}. Data were acquired and analyzed using NETZSCH Proteus software.

QUANTIFICATION AND STATISTICAL ANALYSIS

This study is based on reproducible physical measurements of inorganic polycrystalline samples and does not involve population-based inference. Therefore, no hypothesis-testing statistical analyses (e.g., *p* values, null-hypothesis significance testing) were performed.

For each nominal composition ($x = 0, 0.3, 0.5, 0.7$), one synthesis batch ($\sim$10 g) was prepared ($n = 1$ independent batch per composition). The obtained material was divided into multiple portions and pressed into multiple pellets, which were used as technical replicates for characterization. XRD, electronic transport, thermal expansion, and DSC measurements were performed for all compositions. Magnetization measurements were performed for $x = 0$ and 0.5. NPD and AHE measurements were performed for $x = 0.5$.

Rietveld refinements were performed using GSAS-II, and refinement quality was evaluated primarily using the weighted-profile R factor (R_{wp}) and the goodness-of-fit (GOF). Quantitative parameters (e.g., lattice parameters from refinement; exchange-bias field and coercivity from hysteresis loops; characteristic temperatures from thermal expansion/DSC curves) were extracted following the definitions described in method details and/or the results section.

Because the study does not report averaged values across pellets, individual datasets are presented. Reproducibility was assessed by comparing pellets prepared from the same synthesis batch (technical replicates) and/or repeated measurement cycles on the same specimen, and no formal dispersion measures (SD/SEM/CI) are reported unless explicitly stated in the figure legends and/or the results section. No randomization or stratification procedures were used, and no *a priori* sample-size estimation was performed. No data were excluded unless due to clear instrumental or measurement failure (if applicable). The definition of n, what n represents, and all analysis definitions are provided in the corresponding figure legends and/or the results section.